

A Strategy for Improving the Interfacial Crystallinity and Carrier Mobility of SnO₂ Porous Nanosolids

Chunhong Luan^{1,2}, Chao wang¹, Bao Xu¹, Yujing Geng², Liangmin Zhang³, Qilong Wang⁴, Deliang Cui^{2*}

1 School of Microelectronics and Solid-State Electronics, University of Electric Science and Technology of China, Chengdu 611731, P.R. China

2 State Key Lab of Crystal Materials, Shandong University, Jinan 250100, P.R. China

3 Arkansas Center for Laser Applications and Science, Department of Chemistry and Physics, Arkansas State University, Arkansas 72467, USA

4 Key Laboratory for Special Functional Aggregated Materials of Education Ministry, School of Chemistry & Chemical Engineering, Shandong University, Jinan 250100, P.R. China

Abstract SnO₂ porous nanosolid (PNS) was prepared by a solvothermal hot-press method, and a new strategy was developed to improve its interfacial crystallinity and carrier mobility. It was found that the carrier mobility of SnO₂ PNS was improved after being calcined at 500 °C in high-pressure oxygen. Furthermore, the mobility was greatly increased by calcining SnO₂ PNS at 350 °C for 12 h in high-pressure oxygen, and the highest mobility reached 35 cm²/Vs. On the other hand, the complex impedance spectra of the samples revealed that the annihilation of oxygen vacancies mainly happens within the interfacial region among SnO₂ nanoparticles during the calcinations process in high-pressure oxygen. As a result, the interfacial crystallinity was improved and carrier mobility was increased. Based on the analysis of experimental data, a simple model was proposed to explain the above phenomena. And the simple model may find applications in improving the carrier mobility of other oxide semiconductors used in photovoltaic cells.

Keyword: SnO₂ porous nanosolid; solvothermal hot-press; carrier mobility; high-pressure oxygen calcination.

1. Introduction

Up to now, Grätzel solar cell [1], which is constructed by using TiO₂ nanoparticles as the electron acceptors, possesses the highest photoelectric conversion efficiency. However, there are high density

* Corresponding authors at: State Key Lab of Crystal Materials, Shandong University, Jinan 250100, P. R. China. Tel & Fax: +86-531-88361856, E-mail: cuidl@sdu.edu.cn.

structural defects on the surface of TiO₂ nanoparticles, resulting in the formation of localized state for the charge carriers. These structural defects usually serve as the electron trap centers, decreasing their mobility and resulting in the recombination of electrons and holes. As a result, dark current of the solar cells obviously increases and the photoelectric conversion efficiency decreases accordingly. In order to further improve the performance of solar cells, intensive efforts have been devoted to improving the crystallinity of TiO₂ nanoparticles and searching for alternative oxide semiconductors.

Among the oxides used in solar cells, tin dioxide (SnO₂) is a wide band gap ($E_g=3.6$ eV) n-type semiconductor. Because of its excellent properties, SnO₂ has been widely used in dye-sensitized solar cells [2-7], transparent conducting films [8-10], sensor devices [11-13], field effect transistors etc [14]. When being used in solar cells, SnO₂ should have high crystallinity and electron mobility, so that better photoelectric conversion performance can be achieved. Fortunately, the mobility of SnO₂ is much higher than that of TiO₂ [14-16], thus it is a promising candidate for fabricating high-performance dye-sensitized solar cells. However, due to the fact that SnO₂ used in solar cells is usually in the form of nanoparticles, the interfacial crystallinity among SnO₂ nanoparticles plays an important role in determining the carrier mobility [17]. This result reveals that developing new route to improve the crystalline perfection of interfacial region is very important.

Herein, we find a rule that the carrier of the SnO₂ porous nanosolid (PNS) is related to the calcining atmosphere. As a result, we report a strategy of calcining SnO₂ porous nanosolid (PNS) in high-pressure oxygen, by which both the interfacial crystallinity and carrier mobility of SnO₂ PNS are greatly improved. It is believed that this route may find applications in improving other oxide semiconductors containing oxygen vacancy defect (for example, TiO₂, ZnO, etc), which are also used in photovoltaic cells.

2 Experimental

2.1 Materials

The starting materials used in the experiments were SnO₂ nanoparticles (with particle size of 50~70 nm, purchased from Luoyang Institute of Materials, Henan, China) and dioxane (C₄H₈O₂, A.R.).

2.2 Preparation of SnO₂ porous nanosolid

SnO₂ PNS was prepared by using a solvothermal hot-press (SHP) autoclave (Fig. 1)[18].

Firstly, 3 g SnO₂ nanoparticles were mixed with 5 ml dioxane and ground for 3 h in a planetary ball mill at a rate of 180 rpm. Then the resultant mixture was mounted into the SHP autoclave. When being heated to 100 °C at a rate of 2.5 °C /min, a constant pressure of 60 MPa was applied by the pistons of the autoclave. Afterward, the temperature was further increased at the same rate to 200 °C and kept constant for 3h. After the autoclave was cooled to room temperature, the pressure was released and a green SnO₂ PNS was obtained. By calcining the green SnO₂ PNS at 500 °C in air for 2 h, a well-defined SnO₂ PNS was obtained.

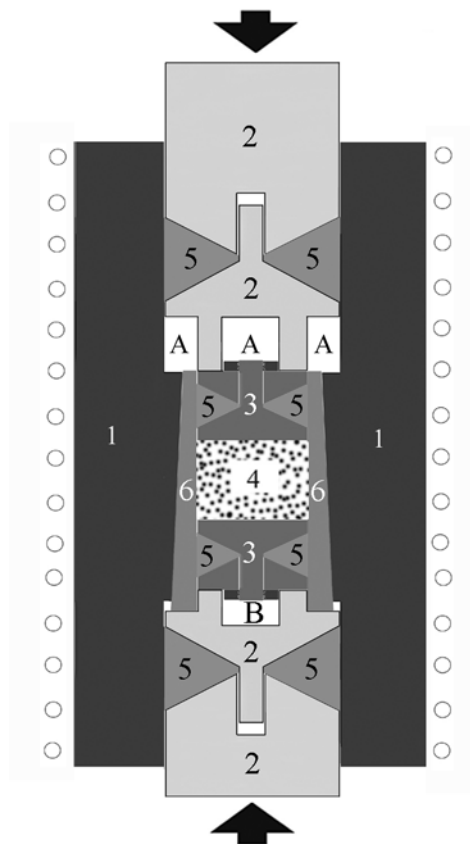


Fig. 1. Schematic diagram of a solvothermal hot-press autoclave.

(1) cylinder, (2) pistons, (3) gaskets, (4) sample, (5) teflon rings, (6) internal cylinder. A and B are the spaces for storing pore-forming solvent

2.3 Characterization of the samples

SnO₂ PNS is an intermediate state between nanoparticles and dense nanoceramics, which possesses both high reactivity of nanoparticles and strength of nanoceramics. The SnO₂ PNS contains interconnected SnO₂ nanoparticles, which form a framework with numerous pores (Fig. 2). Pore size distribution of the SnO₂ PNS was examined on a Quantachrome Pore Master-60 mercury intrusion porosimetry at 20 °C. It is

found that the porosity of SnO₂ PNS is 49.5% and its primary pore diameter is 50~100 nm (Fig. 3). The carrier concentration and mobility of SnO₂ PNS were determined by Hall measurement, which was carried out on an ET9000 series electrical transportation measuring system. Au electrodes were sputter-coated onto the corners of square-shaped samples (7.5×7.5×0.5 mm) in a four-point van der Pauw configuration [19]. Impedance spectroscopy measurements were carried out on an Agilent 4294A & E499A impedance analyzers with overlapping ranges, and the measurement frequency range is 40 Hz~110 MHz. The pellets (with diameter of 23 mm and thickness of 2.5 mm) were sputter-coated with gold electrodes on the opposite surfaces, thereby forming parallel plate capacitor geometry.

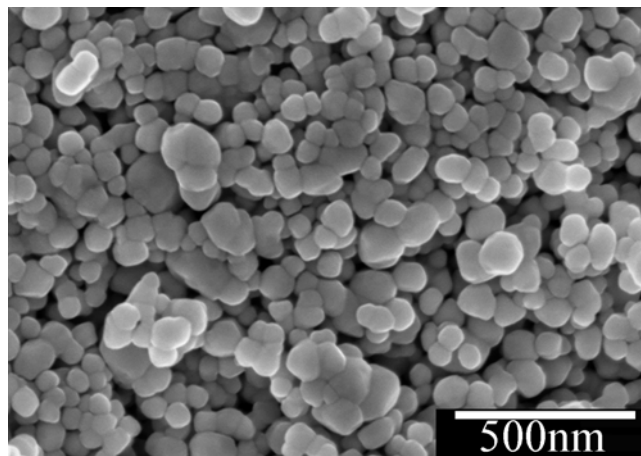


Fig. 2. SEM image of a SnO₂ PNS

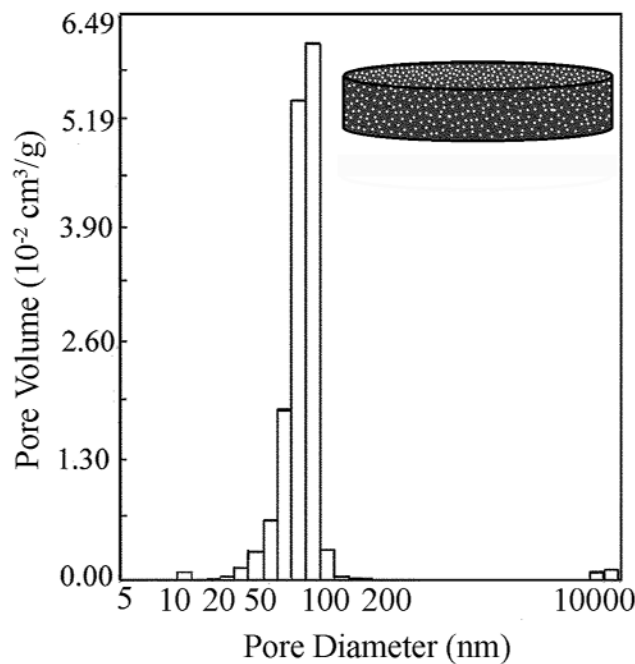


Fig.3 Pore size distribution chart of a SnO₂ PNS

Inset shows the schematic structure of a SnO₂ PNS, white dots denote the pores

3 Results and Discussion

3.1 Modulating carrier mobility of SnO₂ PNS by calcining in different atmospheres

SnO₂ possesses n-type semiconducting characteristic, which is resulted from the oxygen vacancies in SnO₂ nanoparticles. Generally, both the conductivity and carrier mobility of a SnO₂ film/ceramics are mainly determined by the crystallinity of interfacial region, because of the large particle size and comparatively thin depletion layer [20]. Besides, the concentration and distribution of oxygen vacancies in SnO₂ nanoparticles can be modulated by thermal-treatment, and this is especially true within the surface layer of SnO₂ nanoparticles [21, 22]. So, both the concentration and mobility of the carriers can be modulated by calcining SnO₂ in different gases.

Generally, oxygen molecule is chemisorbed at the surface of SnO₂, and it transforms into O₂⁻_{ads} by capturing an electron from SnO₂ below 160 °C. With the temperature further increasing above 160 °C, another electron is captured and O₂⁻_{ads} transforms into O⁻_{ads}. There is a strong tendency for O⁻_{ads} to grab another electron from SnO₂, transforming into O²⁻_{ads} and subsequently becoming lattice oxygen by overcoming Madelung potential [23].

On the basis of the above results, we investigated the effect of calcining in different atmospheres on the mobility of SnO₂ PNSs. In our experiments, the SnO₂ PNSs were calcined at 500 °C for 2 h in air, nitrogen and oxygen, respectively, thus samples A1, A2 and A3 were prepared. As an example, Fig. 4 shows that the I-V curves of sample A1 possess quite good linearity, indicating the homogeneity of this sample and the ohmic contact between the electrodes and SnO₂ PNS.

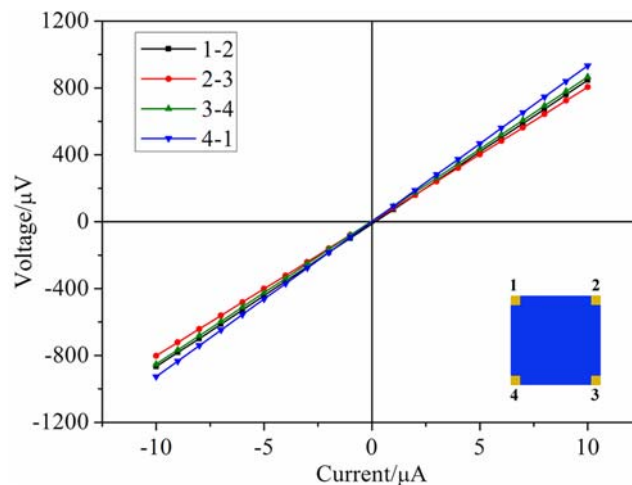


Fig. 4. I-V curves of sample A1

Table 1 shows the results of Hall measurement of samples A1, A2 and A3. Comparing to A1 and A3, sample A2 possesses higher carrier concentration n and lower mobility μ_H . In fact, the SHP process that is used to prepare SnO₂ PNS is completed in a sealed oxygen-deficient space (also see Fig. 1), thus oxygen vacancy defects will inevitably exist both at the surface of SnO₂ nanoparticles and in grain boundaries. Besides, there are large amount of defects in the starting SnO₂ nanoparticles as well. The oxygen vacancies play two important roles, the first role is to provide mobile electrons and making SnO₂ an n-type semiconductor, the second one is to decrease the carrier mobility. When being calcined at 500 °C in N₂, the existing oxygen vacancies in SnO₂ cannot be effectively eliminated, contrarily, more oxygen vacancies can be formed in SnO₂ nanoparticles [24]. The results were also verified in our previous work [25]. As a result, the carrier concentration of sample A2 is quite high and its mobility is low. Compared to A1 and A2, appreciable amount of oxygen vacancies in A3 must have annihilated after being calcined in O₂, resulting in the increase of carrier mobility.

Table 1. Carrier concentration and mobility of SnO₂ PNSs calcined at 500 °C for 2 h in different atmospheres

SnO ₂ PNSs	Atmosp heres	Resistivity (Ω·cm)	$n \times 10^{-17}$ (1/cm ³)	μ_H (cm ² /Vs)
A1	Air	8.52	1.29	5.67
A2	N ₂	2.74	5.83	3.91
A3	O ₂	4.50	2.30	5.98

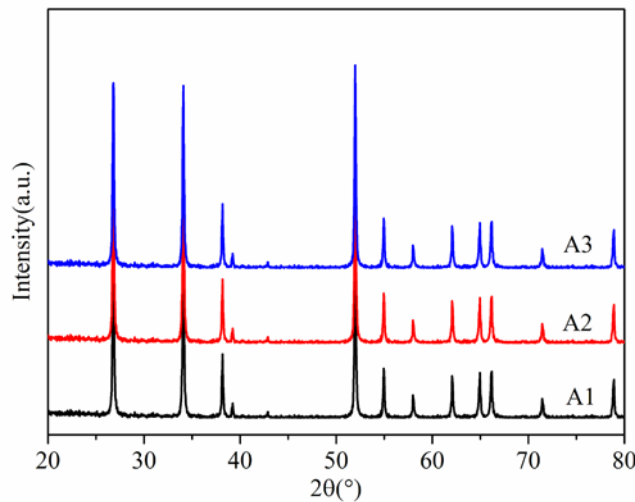


Fig. 5. XRD patterns of samples A1, A2 and A3

In order to understand the mechanism correlated to the above phenomenon, the XRD patterns are presented in Fig.5, and then, the complex impedance spectra of samples A1, A2 and A3 were collected. In Fig.5, all the peaks can be indexed to rutile SnO₂, and no obvious change has been observed after comparing these XRD patterns. This phenomenon suggests that both the phase structure and average particle size of SnO₂ nanoparticles remain unchanged after the calcining process. It means the calcining process might only change the properties of the surface and interface of the SnO₂ PNSs.

In the complex impedance measurement, all the SnO₂ nanoparticles, grains boundaries and the interface between electrode and SnO₂ PNS contribute to the impedance spectra [26]. Besides, the capacitance in the equivalent circuit is often substituted by a constant phase angle element (CPE), which represents the non-ideal capacitance characteristic. Therefore, we proposed an equivalent circuit (RC)(RQ)(RC) (Fig. 6, Q denotes the CPE) for the SnO₂ PNS and fit the measurement results using Zsimp Win 3.10 software.

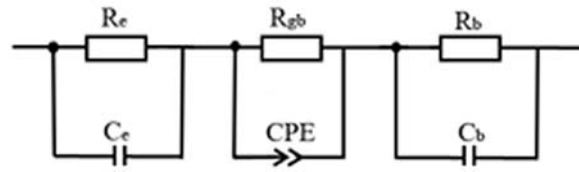


Fig. 6. The equivalent circuit of a SnO₂ PNS

The complex impedance spectra of samples A1, A2 and A3 are shown in Fig. 7, and the fitting results are listed in Table 2. The diameter of SnO₂ nanoparticles D in our samples is 50~70 nm, while the Debye length L_D of SnO₂ is about 3 nm, thus it can be regarded that $D \gg L_D$, so the grain boundary plays a dominating role in the carrier transportation [27, 28]. In fact, the grain boundary resistance (R_{gb}) of SnO₂ PNS remarkably increased after being calcined in air and oxygen. Furthermore, Sample A3, prepared by calcining in oxygen, has the highest R_{gb} , revealing that more oxygen vacancies annihilated in this sample. This phenomenon will inevitably result in the decrease of carrier concentration and increase of depletion layer thickness within the interfacial region [29], which subsequently causes the increase of grain boundary resistance R_{gb} . On comparison, the R_b values of these samples changes much less. This result should be resulted from the fact that the diffusion of oxygen within SnO₂ nanoparticles is much slower than the oxygen exchange reaction on the surface [30].

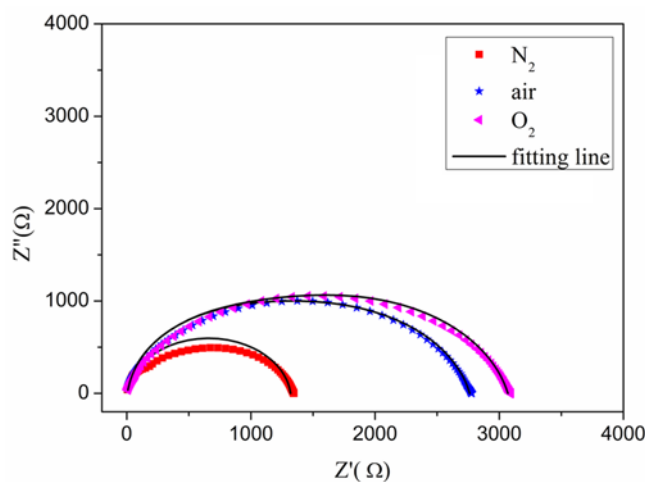


Fig. 7. Impedance spectra of samples A1, A2 and A3

Table 2. Fitting results of impedance spectra of the samples calcined at 500 °C for 2 h in different atmospheres

SnO ₂ PNSs	Atmosphere	R _e (Ω)	R _{gb} (Ω)	R _b (Ω)
A1	air	5.39	2430	1155
A2	N ₂	9.25	1133	594.3
A3	O ₂	6.79	2882	1102

3.2 Increasing the carrier mobility by calcining SnO₂ PNS in high-pressure oxygen

The above results reveal that structural defects within grain boundary in SnO₂ PNS can be restored by calcining in oxygen, thus the carrier concentration decreases and the corresponding mobility increases to some extent. Then what will happen to SnO₂ PNS if it were calcined in high-pressure oxygen? Here we conducted a series of experiments in which SnO₂ PNS was calcined at 500 °C for 2 h under different oxygen pressures. Just as shown in Table 3, the carrier concentration decreases monotonously when the pressure of oxygen increasing from 0.1 MPa to 10 MPa, while the mobility increases from 5.98 to 9.08 cm²/Vs (also see Fig. 8). This result can be attributed to the annihilation of oxygen vacancies and the improvement of crystallinity of the interfacial region among SnO₂ nanoparticles. In fact, accompanying the increase of oxygen pressure, more and more oxygen molecules are chemisorbed on the surface of SnO₂ nanoparticles while SnO₂ PNS is calcined in oxygen. These chemisorbed oxygen molecules will subsequently convert into lattice oxygen by grabbing electrons from SnO₂ nanoparticles, resulting in the improvement of their crystallinity and the annihilation of oxygen vacancies [31]. As a result, the carrier

concentration is decreased and the mobility is improved.

Table 3. Carrier concentration and mobility of SnO₂ PNSs calcined at 500 °C for 2 h in high-pressure oxygen

SnO ₂ PNSs	O ₂ pressure (MPa)	Resistivity (Ω·cm)	$n \times 10^{-17}$ (1/cm ³)	μ_H (cm ² /Vs)
P1	0.1	4.50	2.30	5.98
P2	2.0	4.53	2.25	6.11
P3	4.0	3.89	2.39	6.70
P4	6.0	5.74	1.57	6.94
P5	8.0	7.15	1.14	7.66
P6	10.0	7.16	0.96	9.08

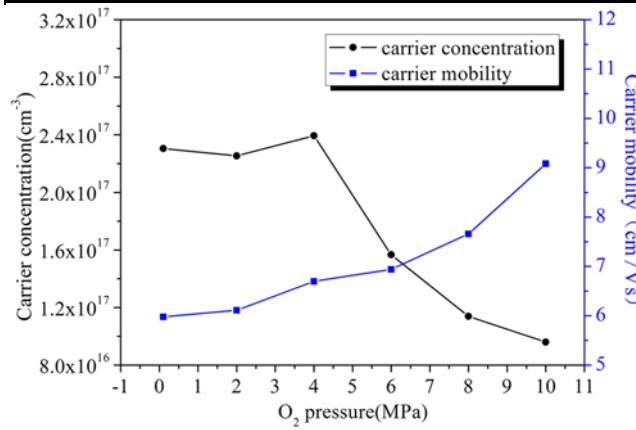


Fig. 8. Variation of carrier concentration and mobility of SnO₂ PNSs

The samples are calcined at 500 °C for 2 h in high-pressure oxygen.

Here the complex impedance spectra of SnO₂ PNSs are used again to analyze the mechanism of the above phenomenon. Fig. 9 presents the impedance spectra of SnO₂ PNSs calcined at different oxygen pressures, and the fitting results of these spectra are shown in Table 4. It can be clearly seen that R_{gb} increases to a large extent with the oxygen pressure increasing from 0.1 MPa to 10 MPa, while R_b changes much less. This result coincides quite well with that of Hall measurement, and it can be explained by the same mechanism mentioned in 3.1.

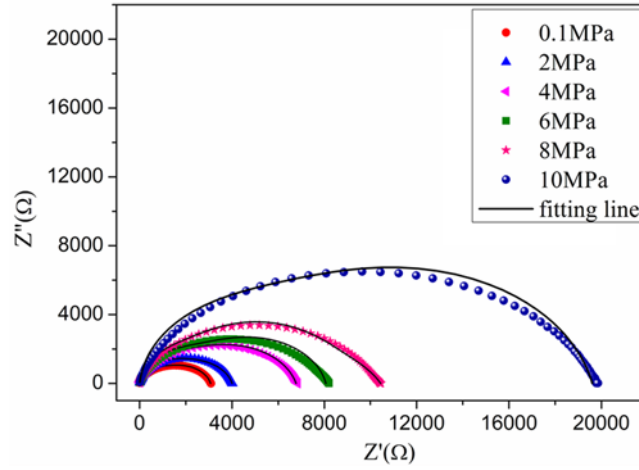


Fig. 9. Impedance spectra of samples calcined at different oxygen pressures

Table 4. Fitting results of impedance spectra of samples calcined at 500 °C for 2 h in high-pressure oxygen

SnO ₂ PNSs	O ₂ pressure (MPa)	R _e (Ω)	R _{gb} (Ω)	R _b (Ω)
P1	0.1	6.79	2882	1102
P2	2.0	7.90	3442	1737
P3	4.0	4.59	5871	2034
P4	6.0	5.47	6770	2186
P5	8.0	7.94	7398	5839
P6	10.0	15.20	19170	6167

3.3 Further increasing the mobility of SnO₂ PNS via low-temperature long-duration calcination

Just as mentioned above, the carrier concentration, hence the conductivity of SnO₂ closely relates to the oxygen vacancies. Furthermore, it is reported that the annihilation of oxygen vacancies in SnO₂ happens at ~350 °C, while the formation of oxygen vacancies appears at much higher temperature [24, 32]. In order to facilitate the annihilation of oxygen vacancies while suppressing their re-generation within SnO₂ nanoparticles, we calcined SnO₂ PNS at 350 °C in high-pressure oxygen for 12 h, thus samples L1, L2, L3, L4, L5, L6 were obtained. The resistivity, carrier concentration and mobility of these samples were evaluated by Hall measurement data, and the results are presented in Table 5 and Fig. 10. Obviously, the mobility exhibits a maximum of 35 cm²/Vs at 4 MPa, which is much higher than that of the samples calcined at 500 °C. On comparison, the carrier concentration decreases monotonically while increasing the oxygen pressure.

Table 5. Carrier concentration and Hall mobility of samples calcined at 350 °C for 12 h in high-pressure

O ₂				
SnO ₂ PNSs	O ₂ pressure (MPa)	Resistivity (Ω·cm)	$n \times 10^{-17}$ (1/cm ³)	μ_H (cm ² /Vs)
L1	0.1	0.73	4.82	17.66
L2	2	0.71	3.77	23.21
L3	4	1.04	1.72	35.00
L4	6	2.77	1.20	18.82
L5	8	8.37	1.29	5.79
L6	10	12.86	1.04	4.88

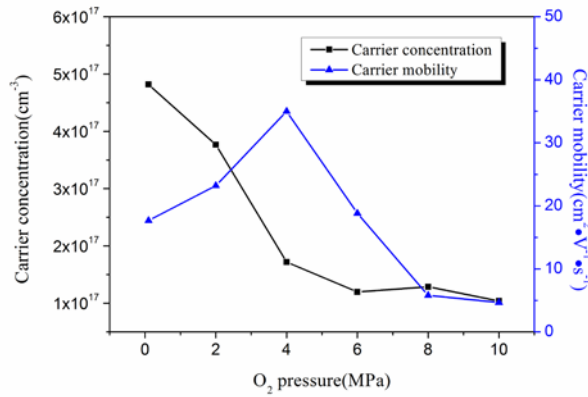


Fig. 10. Carrier concentration and mobility of SnO₂ PNSs calcined at 350 °C for 12 h in high-pressure O₂

It is well known that oxygen vacancies are the major scattering centers for the charge carriers in SnO₂. When being heated at 350 °C in high-pressure oxygen, three processes may have happened within SnO₂ PNS. The first one comprises the diffusion of oxygen vacancies towards the inner part of SnO₂ nanoparticles, thus the distribution of oxygen vacancies becomes more uniform, which decreases the interfacial potential barrier among SnO₂ nanoparticles. The second process includes the annihilation of a certain amount of oxygen vacancies, resulting in the improvement of crystallinity of SnO₂ nanoparticles, especially within the interfacial region [23, 24]. This phenomenon will decrease the interfacial potential barrier and increase the carrier mobility. The third process is that more and more oxygen molecules are chemisorbed on the surface of SnO₂ nanoparticles when the oxygen pressure gradually increasing, grabbing more electrons from SnO₂ nanoparticles and resulting in the thickening of depletion layer. As a result, the migration path of charge carriers becomes narrower [33], and the mobility decreases

accordingly (Fig. 11). All these processes compete with each other, and reach equilibrium at a specific oxygen pressure, for example, 4 MPa in our sample.

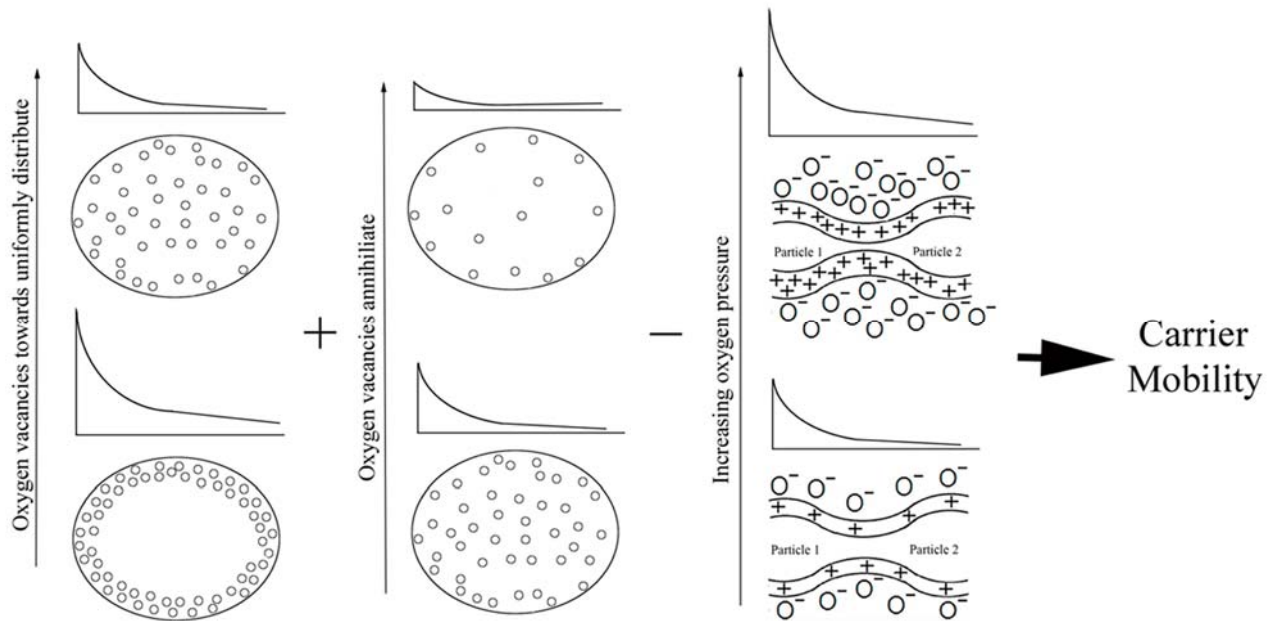


Fig. 11. A schematic diagram of the processes happened in SnO₂ PNS when being calcined in high-pressure oxygen

4 Conclusions

SnO₂ porous nanosolid was prepared using a solvothermal hot-press route, and its carrier mobility was modulated by calcining in different atmospheres. Especially, the mobility of a SnO₂ porous nanosolid greatly increased after being calcined in high-pressure oxygen. Furthermore, by thermal-treating SnO₂ porous nanosolid at 350 °C for 12 h in oxygen of 4 MPa, the mobility greatly increased to 35 cm²/Vs. This phenomenon may find applications in improving the performance of photovoltaic cells based on TiO₂ (SnO₂)/organic dye composite materials.

Acknowledgements

This work is supported by the Natural Science Foundation of China (NSFC 50990061, 51021062, 21073107, 51102151), Natural Science Foundation (ZR2011EMQ002) and Postdoctoral Innovation Foundation (201003077) of Shandong Province, Independent Innovation Foundation (2010TS039) and Postdoctoral Foundation of Shandong University.

References

- [1] B. O'Regan, M. Grätzel, A low-cost, high-efficiency solar cell based on dye-sensitized colloidal TiO₂ films, *Nature* 353 (1991) 737-740.
- [2] X. Dou, D. Sabba, N. Mathews, L.H. Wong, Y.M. Lam, S. Mhaisalkar, Hydrothermal synthesis of high electron mobility Zn-doped SnO₂ nanoflowers as photoanode material for efficient dye-sensitized solar cells, *Chem. Mater.* 23 (2011) 3938-3945.
- [3] E. Ramasamy, J. Lee, Ordered mesoporous SnO₂-Based photoanodes for high-performance dye-sensitized solar cells, *J. Phys. Chem. C* 114 (2010) 22032-22037.
- [4] M.H. Kim, Y.U. Kwon, Semiconducting divalent metal oxides as blocking layer material for SnO₂-based dye-sensitized solar cells, *J. Phys. Chem. C* 115 (2011) 23120-23125.
- [5] N.K. Subbaiyan, E. Maligaspe, F. D'Souza, Near unity photon-to-electron conversion efficiency of photoelectrochemical cells built on cationic water-soluble porphyrins electrostatically decorated onto thin-film nanocrystalline SnO₂ surface, *ACS Appl. Mater. Interfaces* 3 (2011) 2368-2376.
- [6] M.A. Hossain, G.W. Yang, M. Parameswaran, J.R. Jennings, Q. Wang, Mesoporous SnO₂ spheres synthesized by electrochemical anodization and their application in CdSe-sensitized solar cells, *J. Phys. Chem. C* 114 (2010) 21878-21884.
- [7] J. Xing, W.Q. Fang, Z. Li, H.G. Yang, TiO₂-coated ultrathin SnO₂ nanosheets used as photoanodes for dye-sensitized solar cells with high efficiency, *Ind. Eng. Chem. Res.* 51 (2012) 4247-4253.
- [8] H. Kim, C.M. Gilmore, A. Pique, J.S. Horwitz, H. Mattoussi, H. Murata, Z.H. Kafafi, D.B. Chrisey, Electrical, optical and structural properties of indium-tin oxide thin films for organic light-emitting devices, *J. Appl. Phys.* 86 (1999) 6451-6456.
- [9] E.N. Dattoli, Q. Wan, W. Guo, Y. Chen, X. Pan, W. Lu, Fully transparent thin-Film transistor devices based on SnO₂ nanowires, *Nano Lett.* 7 (2007) 2463-2469.
- [10] Y. Huang, Q. Zhang, G. Li, M. Yang, Tungsten-doped tin oxide thin films prepared by pulsed plasma deposition, *Mater. Charact.* 60 (2009) 415-419.
- [11] F. Hernandez-Ramirez, A. Tarancon, O. Casals, J. Arbiol, A. Romano-Rodriguez, J.R. Morante, High response and stability in CO and humidity measures using a single SnO₂ nanowire, *Sens. Actuators, B* 121 (2007) 3-17.
- [12] I. Kocemba, J. Rynkowski, The influence of catalytic activity on the response of Pt/SnO₂ gas sensors

to carbon monoxide and hydrogen, *Sens. Actuators, B* 155 (2011) 659-666.

- [13] Y. Cheng, K.S. Chen, N.L. Meyer, J. Yuan, L.S. Hirst, P.B. Chase, P. Xiong, Functionalized SnO₂ nanobelt field-effect transistor sensors for label-free detection of cardiac troponin, *Biosensors and Bioelectronics* 26 (2011) 4538-4544.
- [14] M.S. Arnold, P. Avouris, Z.W. Pan, Z.L. Wang, Field-effect transistors based on single semiconducting oxide nanobelts, *J. Phys. Chem. B* 107 (2003) 659-663.
- [15] E. Hendry, M. Koeberg, B. O'Regan, M. Bonn, Field effects on electron transport in nanostructured TiO₂ revealed by terahertz spectroscopy, *Nano Lett.* 6 (2006) 755-759.
- [16] Q. Zhang, C.S. Dandeneau, X. Zhou, G. Cao, ZnO nanostructures for dye-sensitized solar cells, *Adv. Mater.* 21 (2009) 4087-4108.
- [17] P. Tiwana, P. Docampo, M.B. Johnston, H.J. Snaith, L.M. Herz, Electron mobility and injection dynamics in mesoporous ZnO, SnO₂, and TiO₂ films used in dye-sensitized solar cells, *ACS Nano* 5 (2011) 5158-5166.
- [18] Q. Yu, K. Wang, C. Luan, Y. Geng, G. Lian, D. Cui, A dual-functional highly responsive gas sensor fabricated from SnO₂ porous nanosolid, *Sens. Actuators, B* 159 (2011) 271-276.
- [19] L.J. van der Pauw, A method of measuring specific resistivity and Hall effect discs of arbitrary shape, *Philips Res. Repts* 13 (1958) 1-9.
- [20] A. Rothschild, Y. Komem, The effect of grain size on the sensitivity of nanocrystalline metal-oxide gas sensors, *J. Appl. Phys.* 95 (2004) 6374-6380.
- [21] J. Getino, J. Gutierrez, L. Ares, J.I. Robla, M.C. Horrillo, I. Sayago, J.A. Agapito, Integrated sensor array for gas analysis in combustion atmospheres, *Sens. Actuators, B* 33 (1996) 128-133.
- [22] A. Oprea, E. Moretton, N. Bârsan, W.J. Becker, J. Wöllenstein, U. Weimar, Conduction model of SnO₂ thin films based on conductance and Hall effect measurements, *J. Appl. Phys.* 100 (2006) 033716, 1-10.
- [23] S. Chang, Oxygen chemisorption on tin oxide: Correlation between electrical conductivity and EPR measurements, *J. Vac. Sci. Technol.* 17 (1980) 366-369.
- [24] D.F. Cox, T.B. Fryberger, S. Semancik, Oxygen vacancies and defect electronic states on the SnO₂ (110)-1×1 surface, *Phys. Rev. B: Condens. Matter* 38 (1988) 2072-2083.

- [25] C. Luan, K. Wang, Q. Yu, G. Lian, L. Zhang, Q. Wang, D. Cui, Improving the gas-sensing performance of SnO₂ porous nanosolid sensors by surface modification, *Sens. Actuators, B* 176 (2013) 475-481.
- [26] A. Labidi, C. Jacolin, M. Bendahan, A. Abdelghani, J. Guerin, K. Aguir, M. Maaref, Impedance spectroscopy on WO₃ gas sensor, *Sens. Actuators, B* 106 (2005) 713-718.
- [27] V. Demarne, A. Grisel, R. Sanjines, D. Rosenfeld, F. Levy, Electrical transport properties of thin polycrystalline SnO₂ film sensors, *Sens. Actuators, B* 7 (1992) 704-708.
- [28] M.W.J. Prins, K.-O. Grosse-Holz, J.F.M. Cillessen, L.F. Feiner, Grain-boundary-limited transport in semiconducting SnO₂ thin films: Model and experiments, *J. Appl. Phys.* 83 (1998) 888-893.
- [29] C. Malagù, M.C. Carotta, A. Giberti, V. Guidi, G. Martinelli, M.A. Ponce, M.S. Castro, C.M. Aldao, Two mechanisms of conduction in polycrystalline SnO₂, *Sens. Actuators, B* 136 (2009) 230-234.
- [30] B. Kamp, R. Merkle, R. Lauck, J. Maier, Chemical diffusion of oxygen in tin dioxide: Effects of dopants and oxygen partial pressure, *J. Solid State Chem.* 178 (2005) 3027-3039.
- [31] S.R. Morrison, *The chemical physics of surfaces*, second ed., Plenum Press, New York, 1990.
- [32] C. Nayral, E. Viala, P. Fau, F. Senocq, J.C. Jumas, A. Maisonnat, B. Chaudret, Synthesis of tin and tin oxide nanoparticles of low size dispersity for application in gas sensing, *Chem. Eur. J.* 6 (2000) 4082-4090.
- [33] M. Ippommatsu, H. Ohnishi, H. Sasaki, T. Matsumoto, Study on the sensing mechanism of tin oxide flammable gas sensors using the Hall effect, *J. Appl. Phys.* 69 (1991) 8368-8374.